High Contrast Imaging of Interphases in Ternary Polymer Blends Using Focused Ion Beam Preparation and Atomic Force Microscopy

Nick Virgilio and Basil D. Favis*

CREPEQ, Department of Chemical Engineering, École Polytechnique de Montréal, Montréal, QC H3C 3A7 Canada

Marie-France Pépin and Patrick Desjardins

Regroupment Québécois sur les Matériaux de Pointe−RMPQ, Department of Engineering Physics, École Polytechnique de Montréal, Montréal, QC H3C 3A7 Canada

Gilles L'Espérance

Center for Characterization and Microscopy of Materials−(CM)², École Polytechnique de Montréal, Montréal, QC H3C 3A7 Canada

Received August 23, 2004; Revised Manuscript Received November 4, 2004

ABSTRACT: In this paper, we demonstrate the applicability of focused ion beam (FIB) preparation followed by tapping mode atomic force microscopy (TMAFM) to analyze model interphase thicknesses in high density polyethylene/polystyrene/poly(methyl methacrylate) (HDPE/PS/PMMA) ternary polymer blends prepared by melt mixing. Previous work has shown that, in a polyethylene matrix, this blend exhibits a dispersed phase composed of a well-segregated PMMA core and a PS shell. Control of the PS/PMMA composition ratio allows for the control of shell thickness and hence this blend provides an excellent model system to analyze interphase thicknesses. A focused ion beam preparation was applied to the melt blended samples to prepare very smooth surfaces without mechanical deformation (i.e., no plowing or interfacial debonding), while TMAFM was used to obtain high-resolution images of the composite droplets in order to measure the mean diameter of the droplets and PS shell thickness. It is shown that the three polymer components have different ion beam etching rates, which results in a topological contrast between the phases of the blends when viewed by tapping mode atomic force microscopy. In this case, PMMA has the highest etching rate, while PS has the lowest and HDPE is intermediate. This high level of contrast between the phases allows for a clear identification of the PS interphase. Even the fine features of particles in the process of coalescing can be clearly identified. To ensure that this procedure was not altering the blend phase sizes in any way, average composite droplet diameters obtained with FIB preparation and TMAFM measurements were compared with the classic technique of cryomicrotome preparation and SEM measurements. The dispersed phase size data from the two procedures compare well. The FIB/TMAFM approach allows for the estimation of the PS interphase thicknesses from 100 to 200 nm depending on the PS/PMMA composition ratio. The approach presented here avoids the pitfalls associated with microtomy such as microvoiding, deformation of the materials and debonding at the interphase. It also eliminates the need for extraction of polymers with selective solvents and staining techniques used to provide contrast. This technique provides significant advantages for the analysis of multicomponent polymer blends or blends with complex morphologies. It also provides a first step toward a new approach for analyzing interphase thickness in polymer blends.

1. Introduction

1.1. Polymer Interphases. Blending polymers is an important approach to develop new high-performance materials arising from synergistic interactions between the constituent polymers[1]. Polymers, when mixed together, form immiscible blends due to thermodynamic considerations. Three key parameters determine the properties of immiscible polymer blends: the properties of the original materials, the morphology of the blends and the interphase (thickness, composition and structure) between the different phases. While morphology has been extensively studied in the past and microscopic characterization conducted with well-established methods, much has still to be done in immiscible melt-processed polymer blends to quantitatively characterize the interphase, or transition region, between the different phases of the blend in terms of thickness, structure and composition.

* To whom correspondence should be addressed. E-mail: basil.favis@polymtl.ca.

Since the early 1970s, theoretical models concerning the interphase thickness and composition profile in immiscible polymer blends have been developed and refined.[2−4] Direct experimental measurements of interphase thickness have mostly been conducted on multilayer polymer films or polymer films deposited on flat polymer substrates using ellipsometry.[5−7] Although ellipsometry is a powerful tool, it is limited to multilayer polymer films with rather large surfaces and with parallel interphases, and is therefore inappropriate for melt-processed polymer blends presenting a very fine dispersed phase of micrometer dimensions.

Direct imaging of the interphase in immiscible melt-processed polymer blends has proven to be quite difficult, mostly due to lack of adequate combinations of sample preparation methods and microscopy techniques. Microtomy and ultramicrotomy are the most commonly used methods to prepare samples for image analysis. However, in many cases, microtomy induces deformation of the material, interfacial debonding be-

10.1021/ma0482664 CCC: $30.25
Published on Web 02/12/2005

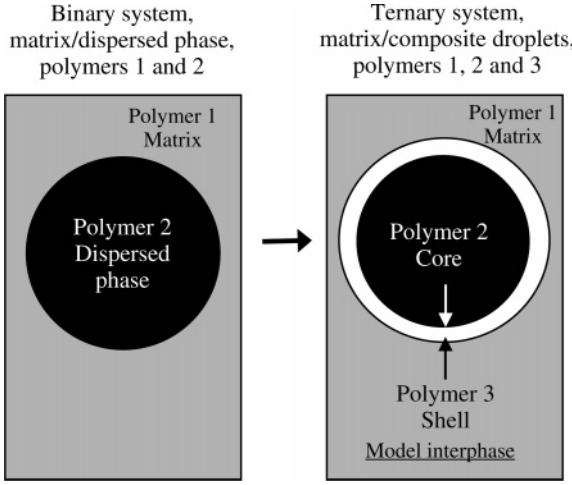

Figure 1. Use of a PS shell as a model interphase.

tween phases and important surface roughness effects. Also, electron microscopy has either insufficient resolution to probe such small regions (SEM) or requires difficult sample preparation methods (TEM).

1.2. Ternary Polymer Blends: Use of a Model Interphase. A first step toward the measurement of the interphase thickness in melt-processed polymer blends would be to measure the thickness of a model interphase (Figure 1), defined here as a discrete phase of different chemical nature located between the matrix and the original dispersed phase of a binary system.

Ternary polymer blends and, more specifically, matrix/composite droplet systems offer this opportunity. The morphology of ternary polymer blends prepared by melt mixing is a result of thermodynamic[8−10] and viscous[11,12] considerations as well as processing conditions.[13,14] Spreading coefficients,[15−18] λ_{ij} (eq 1), give the tendency of component i to spread or encapsulate component j while in a media of component k in order to minimize the interfacial free energy of the overall system.

$$\lambda_{ij} = \gamma_{jk} - \gamma_{ik} - \gamma_{ji} \tag{1}$$

Reignier et al.[19−21] and Guo et al.[18] have extensively investigated HDPE/PS/PMMA ternary blends. They have shown that for blends of 80 vol % HDPE and 20 vol % of PS + PMMA, the system consists of a matrix of HDPE with PMMA/PS core/shell composite droplets, as predicted by the spreading coefficients. By carefully choosing the polymers and processing conditions, all polymers were highly segregated.[20] Control of the processing conditions also resulted in a nearly constant droplet size, while variation of the volume ratio of PS/PMMA allowed for the obtention of PS shells ranging from 200 nm for 50% PS/50% PMMA composite droplets (based on the total dispersed phase volume, which is maintained constant at 20%) to theoretically 20−30 nm thick shells for 14% PS/86% PMMA composite droplets, which is in the range of a molecular layer of PS. Those values were obtained using a simple model based on perfect segregation of the polymers and the size of the dispersed phase.

1.3. Atomic Force Microscopy. AFM[22,23] is a powerful tool to study surface topography and composition of multiphase materials, including composite materials and polymer blends. Tapping mode AFM (TMAFM) has been employed for studying thin films of copolymers and binary polymer blends deposited by solvent casting methods.[24−31] Phase contrast imaging has proven to be a powerful technique to distinguish regions of different chemical natures. A limited number of articles have focused their attention on thin films of immiscible ternary polymer blends using AFM. Walheim et al.[32] have studied 100 nm thick films of immiscible PS/PMMA/poly(2-vinylpyridine) (PVP) blends for a variety of compositions. Using contact mode AFM, they showed that PMMA is located between PS and PVP in order to minimize the interfacial free energy. Furthermore, a variety of morphologies can be obtained, depending on the relative composition of blend constituents. Finally, the surface polarity of the substrate has an important effect on the resulting morphology. While a nonpolar surface results in a planar film structure, a polar surface results in a 3-D film structure, which again minimizes surface free energy. Cyganik et al.[33] studied 30−90 nm thick films of deuterated PS (dPS)/PMMA/PVP at a 2:1:2 weight composition ratio using contact and lateral (friction) mode AFM. This latter mode of analysis is related to tip−sample adhesion, which is characteristic of the material's nature. It is therefore a route to obtain chemical information on a heterogeneous surface. They obtained similar results to those of Walheim, in which PMMA situates itself between PS and PVP.

In addition to thin film study, there are also some reports on AFM investigations related to melt mixed polymer blend microstructures.[34,35] Blends of polypropylene (PP) with a compatible copolymer (such as ethylene−propylene (EP)) offer good interfacial and mechanical properties that permit micrometer and nanometer-scale structure investigations with AFM.[36−40] Investigation of the EP dispersed phase reveals a complex structure presenting amorphous and crystalline regions of different chemical natures. Galuska et al.[41] studied a variety of bulk polymer blends using AFM and samples prepared by microtomy. Force modulation AFM was used to map the elastic properties of the materials. PP/EP blends and PP/EPDM blends with different amounts of cross-linked EPDM were characterized. In the latter case, it was possible to distinguish the different degrees of cross-linking of EPDM, something that is impossible to observe with SEM and TEM. Pfau et al.[42] also used force modulation AFM to map elastic properties for a variety of polymer blends, among which were rubber toughened PP and high-impact polystyrene (HIPS). Their images of HIPS, which possesses a matrix/composite droplet morphology, permitted the observation of 30−40 nm thick polybutadiene shells around the PS cores. They also showed that the TEM and AFM provide similar results concerning the microstructure. HIPS is a well adapted blend for microtomy and AFM analysis. However, this is not the general case for polymer blends.

One of the major problems with AFM characterization of melt-processed polymer blends is the surface preparation using microtomy, which can induce artifacts on AFM images caused by deformation of the materials, important surface roughness and interfacial debonding. This problem has been one of the most important limitations for the applicability of AFM to the study of polymer blend interphases.

1.4. Focused Ion Beam Preparation. The focused ion beam technique is a recently developed tool that allows one to prepare samples for microscopic observation. It is a physical process that permits the preparation of surfaces with an ion beam, most commonly

Table 1. Properties of the Materials

	M_w[a] $\times 10^{-3}$ g/mol	M_n[a] $\times 10^{-3}$ g/mol	melt index[b] ASTM g/10 min	density,[b] g/cm^3		η^* x 10^{-3} Pa.s (at 200 °C)		N1 $\times 10^{-4}$ Pa (at 200 °C)	
				20 °C	200 °C	$\dot{\gamma}^c$	τ^d	$\dot{\gamma}^c$	τ^d
HDPE	79	24	4	0.96	0.75	1.2	1.2	2.2	2.2
PS	290	141	15	1.04	0.97	1.7	2.6	11	5.1
L-PMMA	11.9	7.8			1	0.04	0.04	0.02	0.6

[a] Measured by GPC. [b] Obtained from supplier. [c] Average shear rate during blending: $\dot{\gamma} = 25\ s^{-1}$. [d] Average shear stress during blending: $\tau = 2.7 \times 10^4$ Pa.

gallium ions, with a typical energy of 30 keV. The beam scans and gradually etches the selected surface due to collisions of the ions with the material. By controlling the beam current and energy, the scanning speed and exposition time, it is possible to obtain very precise structures. This approach, contrary to microtomy, does not induce mechanical stresses on the sample. However, the surface treatment of polymers using high energy ions or radiation is known to cause amorphization of the sample surface,[43−45] scission and/or cross-linking of polymer chains,[46−53] shrinkage of chains,[54] and modification of the surface chemistry.[55−60] FIB sample preparation has mainly been used with metallic and semiconducting materials. Few papers have studied the effect of FIB treatment on polymer surfaces,[61−63] and none on melt-processed polymer blend surfaces. However, the combination of plasma etching of polymer surfaces and microscopic surface analysis has proven to be a very useful tool to study thin film surface and volume morphology.[64,65]

The objective of this work is to examine the potential of combining focused ion beam preparation and atomic force microscopy to examine polymer blend interphases. A polymer blend comprised of a core/shell dispersed phase will be used as a model system.

2. Experimental Procedures

2.1. Materials. Ternary blends of HDPE, PS, and PMMA were prepared with high-density polyethylene 4352 N and polystyrene 615 APR, both obtained from the Dow Chemical Company. Poly(methyl methacrylate) 20 033-6 was obtained from Aldrich. Interfacial tensions and spreading coefficients were obtained previously using the breaking thread method.[20] These materials were chosen so that very high levels of segregation of the homopolymers were obtained. The material characteristics are given in Table 1, where η^* is the complex viscosity and N1 is the first normal stress difference. Both η^* and N1 are measured at constant shear rate and constant shear stress.

2.2. Blend Preparation. Melt mixing was carried out in a 50 mL Haake Rheocord 90 chamber at 50 rpm and 200 °C for 8 min. A small amount (0.2 wt %) of Irganox B225 antioxidant from Ciba-Geigy was added to the blend to reduce thermal oxidation of polyethylene. After mixing, samples from the blends were immediately cut and plunged into a bath of water at ambient temperature to freeze-in the morphology.

2.3. Morphological Analysis: Scanning Electron Microscopy. The specimens were cryogenically cut to obtain a planar face using a microtome RM 2165 from Leica equipped with glass knives. Samples and knives were cooled to −160 °C before microtomy was performed. Polystyrene was selectively dissolved with cyclohexane at room temperature for 1 day. Samples were then plasma coated with a gold−palladium layer under pulse mode for 20 min. Morphological observations were carried out with a JEOL JSM 840 scanning electron microscope operated at a voltage of 15 kV.

2.4. Focused Ion Beam Sample Preparation. Specimens were first cryomicrotomed (see previous section) and then plasma-coated (see previous section). The focused ion beam (FIB) surface preparation was then performed with a Hitachi FIB-2000A using a 30 keV Ga^+ beam. Focused ion beam consists of a liquid metal ion source (LMIS), generally gallium, Ga, which emits ions when subjected to a high voltage. Since this high potential is relative to a nearby electrode, the liquid metal assumes a conical shape and evaporation takes place at its apex. A flow of Ga coming from a nearby reservoir replaces the evaporated atoms. The atoms that evaporate are ionized, producing the Ga^+ ions. Since the emitting area is small, it is possible to focus the ion beam on a very small spot, resulting in a high resolution. Using a system of electromagnetic lens and diaphragms, it is possible to control the beam size, the intensity, and the area scanned. The beam current was set at approximately 0.8 nA and the dwelling time at 3 μs. A layer of approximately 3−4 μm thick was removed by milling parallel to the observed surface, as shown in Figure 2a, on a 80 μm × 3−4 μm section for approximately 8 h, with a fluence rate of approximately 1.8×10^{15} ions/cm^2/s.

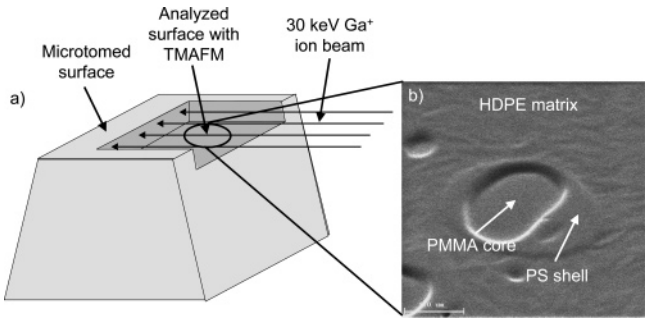

Figure 2. (a) Surface preparation using focused ion beam and (b) 4 μm × 4 μm scanning ion microscope (SIM, within the FIB instrument) micrograph of the resulting surface prepared with focused ion beam on a 80% HDPE/10% PS/10% PMMA blend.

2.5. Morphological Analysis: Atomic Force Microscopy. Morphological observations of specimens prepared with the focused ion beam were carried out with a scanning probe microscope Dimension 3100 with a Nanoscope IIIa controller from Veeco Instruments. Silicon tips, model RTESP from Veeco, with spring constants of 20−80 N/m and resonant frequency of approximately 320 kHz were used. The tip was oscillated at approximately 98% of the resonant frequency and the engagement on the surface was done at 95% of the free oscillation amplitude. Topographical pictures were taken at 95% of the free oscillation amplitude. Specimens were fixed on a metallic support using silver glue or graphite tape.

2.6. Image Analysis and Average Diameter Measurements. Images obtained with SEM and AFM were used to quantify the morphology. Images were analyzed using a digitizing table from Wacom. Approximately 150 particles were used to evaluate the volume average diameters D_v of composite droplets using AFM images, and approximately 600 using SEM images. Since microtomy and focused ion beam preparation do not necessarily cut spheres at the equator, and to account for polydispersity effects, the Saltikov correction[66] procedure was applied in order to obtain corrected values of D_v. Average shell thicknesses were obtained by measuring the PS shells directly on the AFM images. Four measurements were taken for each analyzed composite droplet. The average thickness values were obtained by simply averaging the measurements taken for each composition, with an estimated error of 5% for thick shells and 10% for the thin ones.

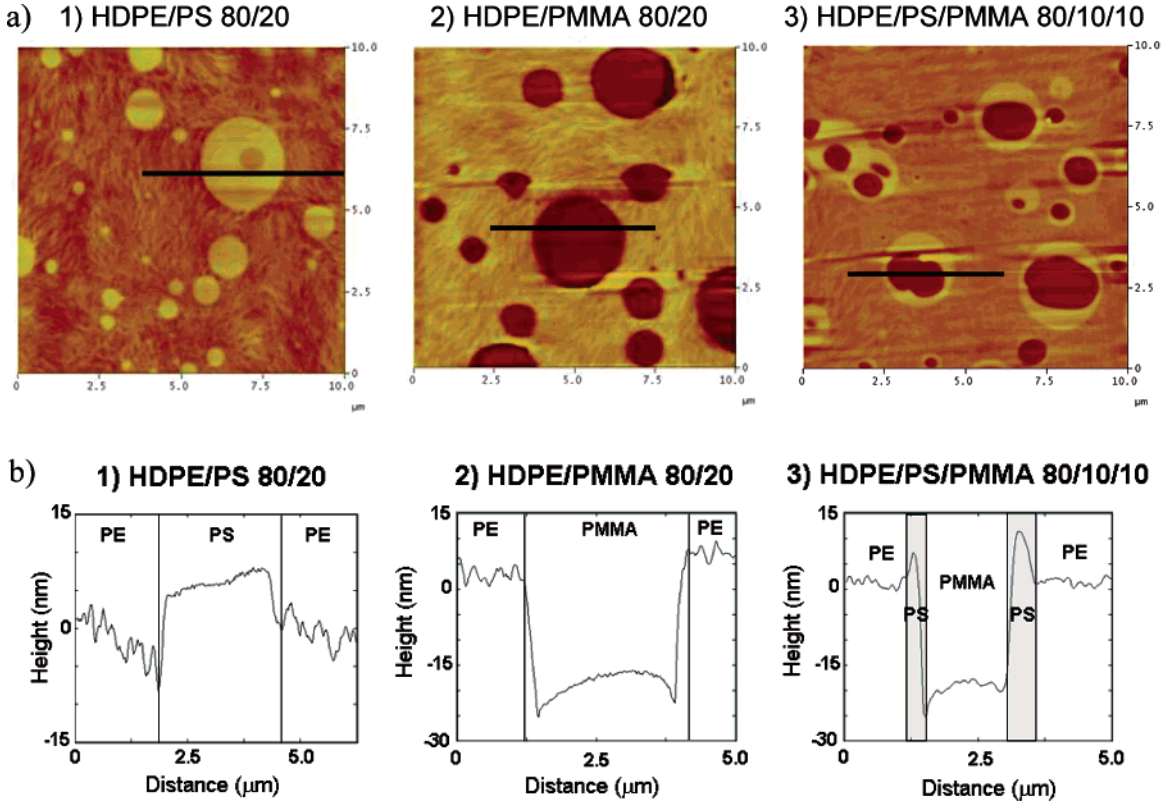

Figure 3. (a) TMAFM topographical surface images of (1) 80% HDPE/20% PS, (2) 80% HDPE/20% PMMA and (3) 80% HDPE/10% PS/10% PMMA. Pictures were taken at 95% of the free oscillation amplitude A_0, scan sizes are 10 μm × 10 μm. (b) TMAFM corresponding sections of (1) 80% HDPE/20% PS, (2) 80% HDPE/20% PMMA, and (3) 80% HDPE/10% PS/10% PMMA.

3. Results and Discussion

3.1. Sample Preparation Using Focused Ion Beam. Before the focused ion beam preparation, cryomicrotomy was performed in order to obtain a relatively flat and straight surface. Alignment of the surface and the Ga^+ ion beam was performed manually, with particular attention to ensure that the beam and surface are parallel to each other. Since it is important to avoid thermal damage of the sample as much as possible, a relatively low fluence rate was used. Surface analysis after FIB preparation reveals a wavelike structure perpendicular to the incident beam direction. This effect is due to the shape of the beam and operating parameters. These waves are relatively equidistant to each other (1.5 μm peak to peak), and their amplitudes are approximately equal to 50 nm. The scanning ion microscope analysis reveals that this approach results in no interfacial debonding (as opposed to microtome preparation) and no mechanical deformation (Figure 2b).

3.2. AFM Morphological Analysis of Samples Prepared with Focused Ion Beam: Binary Blends and Determination of Etching Rates. To clearly identify and calibrate the observed features in ternary blends prepared with FIB and analyzed with AFM, we first investigated binary blends of 80% HDPE/20% PS and 80% HDPE/20% PMMA. Previous studies with SEM[19] showed that both these systems consist of a HDPE matrix with PS or PMMA dispersed phases, respectively. After FIB treatment and AFM analysis, similar morphologies were observed, as shown in Figure 3.

The first image in Figure 3a shows the morphology of the 80% HDPE/20% PS blend. It can be seen that PS is etched less rapidly than HDPE, leading to a height difference between HDPE and PS of approximately 10 nm, as shown on the corresponding profile of Figure 3b. This difference can further be enhanced after the initial FIB preparation by milling the surface with a 30 keV Ga^+ ion beam perpendicular to the surface at a fluence rate of 1.8×10^{15} ions/cm^2/s for no more than a couple of minutes. The HDPE/PMMA blend also exhibits a distinct topography, but in that case PMMA is milled more than HDPE, leading to a height difference between HDPE and PMMA of approximately 25 nm, as shown in the second image of Figure 3a and by the second profile in Figure 3b. Again, this difference can be further enhanced by exposing the surface to a perpendicular Ga^+ ion beam. A high level of contrast between the different polymer domains is thus obtained as a result of differences of topography levels, which results from differences in apparent etching rates. Under these experimental conditions, the apparent etching rates of HDPE, PS and PMMA are, in decreasing order:

$$\text{PMMA} > \text{HDPE} > \text{PS}$$

From previous work, it is known that ternary blends of HDPE/(PS + PMMA) consist of a HDPE matrix with dispersed composite droplets, with PS encapsulating PMMA. Maintaining the same FIB preparation parameters for ternary blend surface preparation as above, it is expected that AFM imaging will show higher topography for PS, which forms the skin or shell of the composite droplet, while PMMA, forming the core, will show lower topography and HDPE level will be between the other two. The third image of Figure 3a confirms these predictions. As can be seen on the corresponding section in Figure 3b, we pass from a midlevel section, corresponding to the HDPE, to a higher region, which corresponds to the PS shell and then to a low-level region, which is the PMMA. We then pass again in the

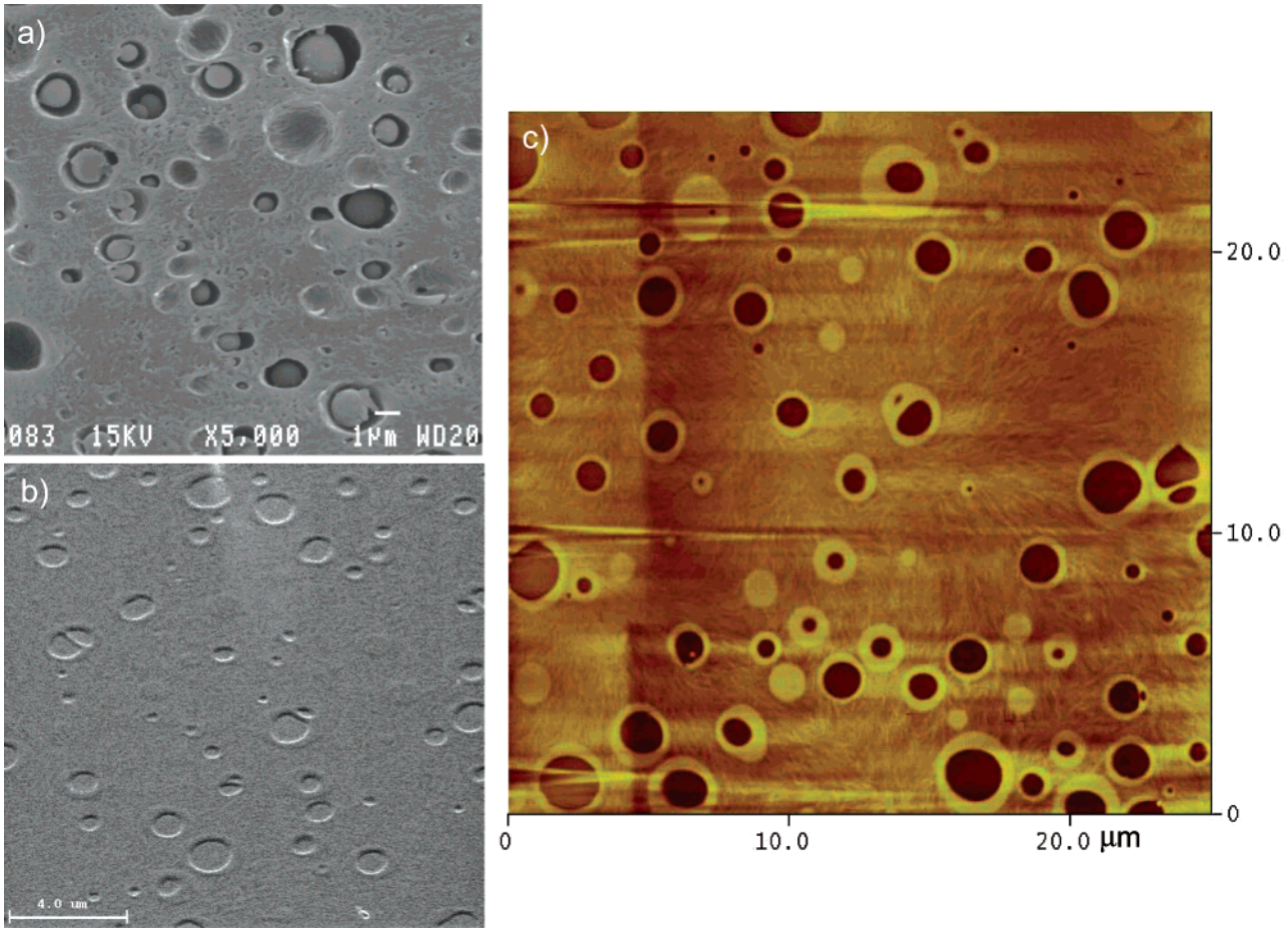

Figure 4. Comparison between (a) SEM surface micrograph of 80% HDPE/10% PS/10% PMMA, prepared by cryomicrotomy and PS extraction using cyclohexane, (b) Scanning ion microscope (SIM) surface micrograph of 80% HDPE/10% PS/10% PMMA prepared by cryomicrotomy and FIB, and (c) TMAFM image of 80% HDPE/10% PS/10% PMMA prepared by cryomicrotomy and FIB.

PS region and return to the HDPE. The qualitative features of the blends are then compared to what is observed with microtome/SEM imaging. Figure 4a shows the morphology of a HDPE/PS/PMMA blend as seen with SEM (microtomy and PS extracted), while Figure 4b shows the same blend using the scanning ion microscope (FIB preparation, no extraction). Figure 4c, once again, shows the high level of topographical contrast when using FIB and AFM analysis. Even the fine features of particles in the process of coalescing can be clearly identified. It can be seen that the structures are qualitatively similar.

Clearly, different polymers react differently when exposed to a 30 keV Ga^+ ion beam, and these differences are reflected in the final topography of the milled surface, revealing the morphology of the blend. High energy ion bombardment of polymers induces physical and chemical modifications of the materials.

At low and medium fluences, it has been reported that PS mainly undergoes cross-linking,[45,49−53] while PMMA first undergoes chain scission[45−48] (accompanied by gas generation and diffusion through the surface) and then cross-linking.[46] Both of these reactions result in a volume decrease. Since both cross-linking and scission have been reported for PMMA while only cross-linking is observed for PS, this could explain why PS domains are less etched than PMMA ones. The third polymer, HDPE, has domains situated topographically between those of PS and PMMA. At low fluences, HDPE, a highly crystalline polymer, first undergoes amorphization and cross-linking.[45,58] Furthermore, it has been reported that PE has a higher cross-linking yield than PS[45] which could explain why HDPE is topographically lower than PS. Also, since PE does not undergo chain scission, this could potentially explain why it is still topographically higher than PMMA. A detailed study on etching mechanisms will be necessary in order to clearly understand etching rates.

At high ion dose, polymers undergo major chemical modifications through loss of matter (gas generation[57]), cross-linking, and/or scission. Their properties are significantly modified and they tend to form amorphous carbon compounds rich in hydrogen (referred as graphitization or carbonization).[58−60] As a result, chemical and physical differences can decrease. This could explain why, after FIB treatment, TMAFM phase contrast is not observed in our experiments.

This approach could be a significant advantage for studying polymer blend morphology when selective extraction of a polymer and classic SEM analysis is impossible. Furthermore, parts a and b of Figure 4 show that surface roughness after FIB preparation is negligible compared to microtomy preparation. In addition, no deformation of the materials occurs and no interfacial debonding is observed. Elimination of these preparation issues makes the observation of the interphase in immiscible polymer blends more accessible.

3.3. FIB Preparation and AFM Microscopy of Ternary Blends: Comparison with Classical Microtomy/SEM Method. In this part of the work we will

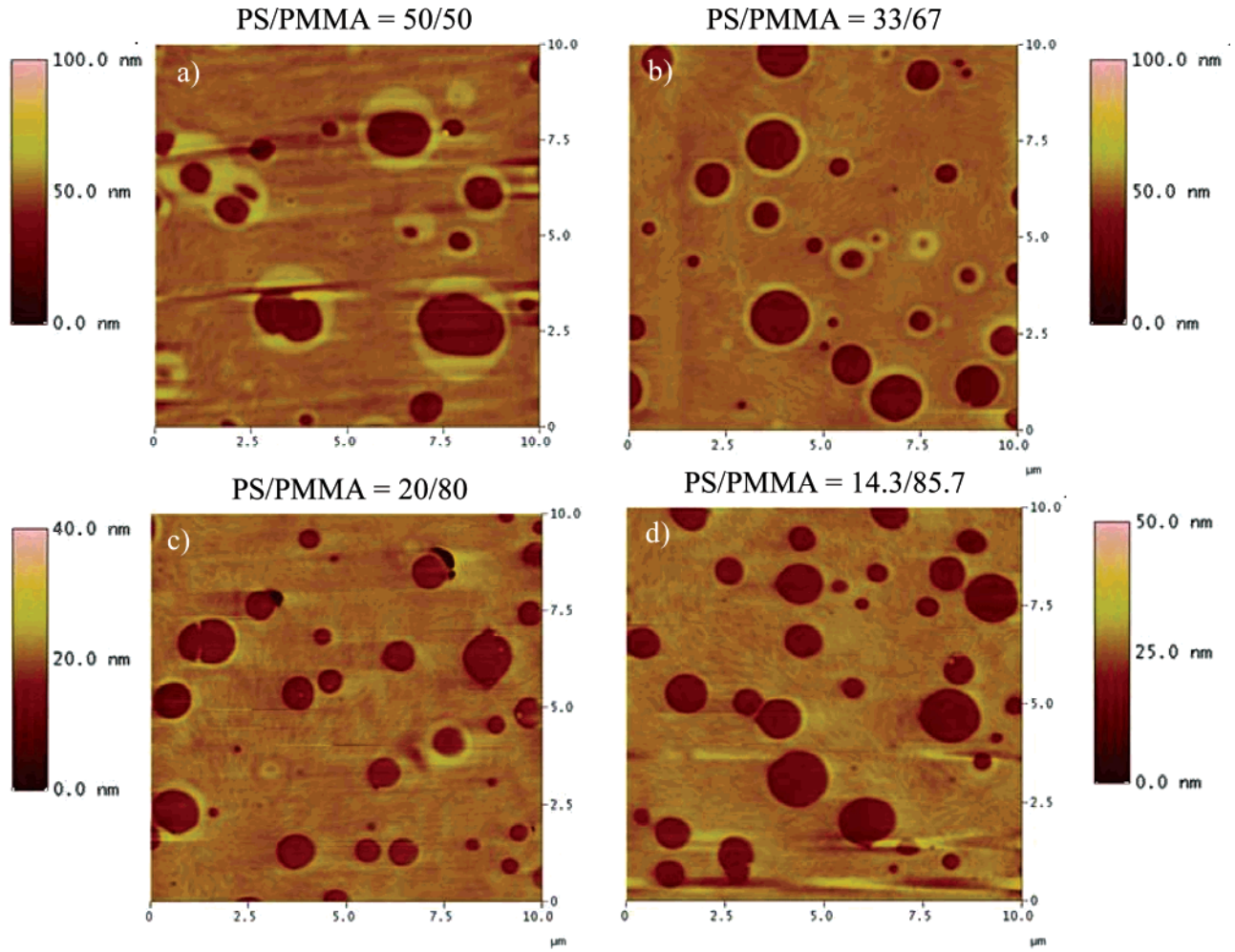

Figure 5. TMAFM surface images of 80% HDPE/20%(PS + PMMA) at different PS/PMMA ratios. Pictures were taken at 95% of the free oscillation amplitude A_0, scan sizes are 10 μm × 10 μm. Topographical height scales also shown beside images.

compare the mean diameters and shell thicknesses of 80% HDPE/20%(PS + PMMA) ternary polymer blends with SEM results. By varying the PMMA/PS volume ratio (for a total constant dispersed phase content of 20 vol %), it is possible to vary the PS shell thickness (our model interphase). Four ternary blends with different PMMA/PS volume ratios were analyzed: 1, 2, 4 and 6, plus binary blends of 80% HDPE/20% PS and 80% HDPE/20% PMMA. Samples of each composition were prepared with FIB and analyzed with AFM. Figure 5 shows topographical AFM images of the four ternary blend compositions that were analyzed.

As the composition in PS decreases, it can be seen that the PS shell thickness also decreases, while the composite droplets mean diameter does not change significantly with PMMA/PS ratio. This effect was also observed previously.[20] Figure 6 shows the volume average diameters D_v obtained with SEM and AFM analysis. Overall, the results are quite similar.

It can be seen that PS acts as a low-level emulsifier for the HDPE/PMMA system, decreasing the average size of the composite droplets. The minimum diameter is obtained for composite droplet compositions near 20% PS/80% PMMA. The initial decrease and subsequent increase of composite droplet diameter as a function of PS content is a result of the competition between an initial decrease of the interfacial tension (reducing the droplet size) and a subsequent increase of the viscosity ratio (increasing the droplet size), as explained by

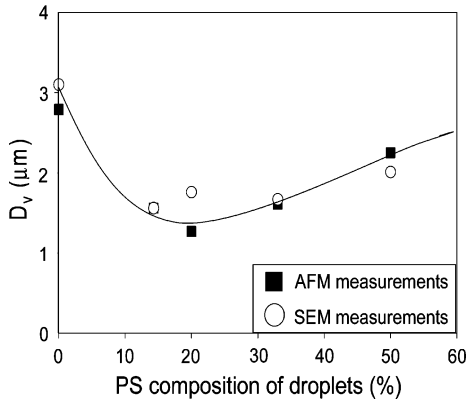

Figure 6. Volume average diameter D_v of composite droplets for 80% HDPE/20%(PS + PMMA) blends with different PS content of composite droplets.

Reignier et al.[20] FIB preparation and AFM analysis permit one to clearly observe all the droplets present at the sample surface, including the very small ones.

3.4. Quantitative Measurement of the PS Shell Thickness. Following the measurements of the volume average diameters, it is of interest to measure the PS shell thickness as a function of PS content of the composite droplets. Using the classic microtomy/extraction/SEM procedure or even TEM analysis, material deformation and interfacial debonding often seriously interfere with interphase imaging. With FIB prepara-

Table 2. Thicknesses of PS Shells (AFM results) for 80% HDPE/20%(PS + PMMA) Blends

composition PS/PMMA	D_v of composite droplets (μm) $\pm$ 0.1 μm	thickness of the shell (nm)
50/50	2.2	198
33/67	1.6	143
20/80[a]	1.4	103

[a] Limiting case. Droplets measured only in the case where shells are clearly visible on the AFM images.

tion and AFM analysis, progressing from part a to part c in Figure 5, one clearly observes a decrease of the PS shell thickness with decreasing PS content. In Figure 5d, it becomes more difficult to distinguish the PS shell phase. The shell thickness was determined in a straightforward fashion by measuring it directly on the AFM images, as described in the Experimental Section. Table 2 shows the average shell thickness for 50% PS/50% PMMA, 33% PS/67% PMMA and 20% PS/80% PMMA composite droplets.

The average shell thickness decreases from 198 nm for the first composition, to 143 nm for the second composition and finally to 103 nm for the third one. Also, in the 20% PS/80% PMMA case, the shell is so thin that we had to choose particles for which the shell was visible on the images. This selection method neglects the very thin shells and overestimates the average thickness. In all three cases, no correction was applied for the polydispersity effect and for the fact that the composite droplets are not necessarily cut at the equator. However, the shells are thin enough so that the corrections related to the measurements should be relatively small. Even if it is more difficult to see the PS shells for the 20% PS/80% PMMA and the 14.3% PS/85.7% PMMA compositions, it is still possible to see it in many cases. Also, a decrease in shell thickness is apparent between the two. It was difficult to experimentally measure the shell thicknesses for composite droplets with PS content inferior to 20%. In that case, the topographical contrast does not sufficiently resolve such small structures. Also, the FIB surface treatment can result in a certain loss of phase contrast, which is related to tip−sample interactions and the nature of the materials.

4. Conclusion

We demonstrate a novel approach for the analysis of model interphases in immiscible ternary polymer blends using focused ion beam (FIB) preparation followed by tapping mode atomic force microscopy (TMAFM). A model 80% HDPE/20%(PS + PMMA) ternary blend, comprised of a HDPE matrix and a dispersed phase with a PS shell and a PMMA core was used. Shell thicknesses can be readily controlled in such a system by varying the PS/PMMA composition ratio. It is shown that the three polymer components have different ion beam etching rates, which results in a topological contrast between the phases of the blends when viewed by tapping mode atomic force microscopy. This high level of contrast allows for a clear identification of the PS model interphase. Even the fine features of particles in the process of coalescing can be clearly identified. Subsequent image analysis allows for an estimation of the model interphase thickness with values ranging from 100 to 200 nm depending on the PS/PMMA composition ratio. This novel technique eliminates difficulties in morphology sample preparation such as debonding due to microtomy and the necessity of staining or solvent etching to improve contrast and provides a new approach toward the analysis of interphase thickness in polymer blends.

Acknowledgment. The authors thank Mr Eric Duchesne and Mr Philippe Plamondon, from the Center for Characterization and Microscopy of Materials ((CM)^2) of École Polytechnique de Montreal, for their assistance with the preparation of samples using the FIB.

References and Notes

(1) Polizu, S.; Favis, B. D.; Vu-Khanh, T. *Macromolecules* **1999**, *32*, 3448−3456.
(2) Helfand, E.; Tagami, Y. *J. Polym. Sci., Part B* **1971**, *9*, 741−746.
(3) Helfand, E.; Tagami, Y. *J. Chem. Phys.* **1972**, *56*, 3592−3601.
(4) Broseta, D.; Fredrickson, G. H.; Helfand, E.; Leibler, L. *Macromolecules* **1990**, *23*, 132−139.
(5) Yukioka, S.; Nagato, K.; Inoue, T. *Polymer* **1992**, *33*, 1171−1176.
(6) Yukioka, S.; Inoue, T. *Polymer* **1993**, *34*, 1256−1259.
(7) Kressler, J.; Higashida, N.; Inoue, T.; Heckmann, W.; Seitz, F. *Macromolecules* **1993**, *26*, 2090−2094.
(8) Vanoene, H. *J. Colloid Interface Sci.* **1972**, *40*, 448−467.
(9) Berger, W.; Kammer, H. W.; Kummerlöwe, C. *Makromol Chem.* **1984**, *Suppl. 8*, 101−108.
(10) Legros, A.; Carreau, P. J.; Favis, B. D.; Michel, A. *Polymer* **1997**, *38*, 5085−5089.
(11) Gupta, A. K.; Srinivasan, K. R. *J. Appl. Polym. Sci.* **1993**, *47*, 167−184.
(12) Nemirovski, N.; Siegmann, A.; Narkis, M. *J. Macromol. Sci.—Phys.* **1995**, *B34*, 459−475.
(13) Favis, B. D.; Chalifoux, J. P. *Polymer* **1988**, *29*, 1761−1767.
(14) Favis, B. D.; Lavallée, C.; Derdouri, A. *J. Mater. Sci.* **1992**, *27*, 4211−4218.
(15) Torza, S.; Mason, S. G. *Colloid Sci.* **1970**, *33*, 67−83.
(16) Hobbs, S. Y.; Dekkers, M. E.; Watkins, V. H. *Polymer* **1988**, *29*, 1598−1602.
(17) Harkins, W. D. *The Physical Chemistry of Surface Films*; Reinhold Pub. Co.: New York, 1952, p 23.
(18) Guo, H. F.; Packirisamy, S.; Gvozdic, N. V.; Meier, D. J. *Polymer* **1997**, *38*, 785−794.
(19) Reignier, J.; Favis, B. D. *Macromolecules* **2000**, *33*, 6998−7008.
(20) Reignier, J.; Favis, B. D. *AIChE J.* **2003**, *49*, 1014−1023.
(21) Reignier, J.; Favis, B. D.; Heuzey, M.-C. *Polymer* **2003**, *44*, 49−59.
(22) Binnig, G.; Quate, C. F.; Gerber, C. *Phys. Rev. Lett.* **1986**, *56*, 930−934.
(23) Zhong, Q.; Inniss, D.; Kjoller, K.; Elings, V. B. *Surf. Sci.* **1993**, *290*, L688-L692.
(24) Kajiyama, T.; Tanaka, K.; Ohki, I.; Ge, S.-R.; Yoon, J.-S.; Takahara, A. *Macromolecules* **1994**, *27*, 7932−7934.
(25) Motomatsu, M.; Mizutani, W.; Tokumoto, H. *Polymer* **1997**, *38*, 1779−1785.
(26) McLean, R. S.; Sauer, B. B. *Macromolecules* **1997**, *30*, 8314−8317.
(27) Bar, G.; Thomann, Y.; Brandsch, R.; Cantow, H.-J.; Whangbo, M.-H. *Langmuir* **1997**, *13*, 3807−3812.
(28) Bar, G.; Thomann, Y.; Whangbo, M.-H. *Langmuir* **1998**, *14*, 1219−1226.
(29) Bar, G.; Brandsch, R.; Whangbo, M.-H. *Langmuir* **1998**, *14*, 7343−7347.
(30) Raghavan, D.; VanLandingham, M.; Gu, X.; Nguyen, T. *Langmuir* **2000**, *16*, 9448−9459.
(31) Budkowski, A.; Bernasik, A.; Cyganik, P.; Raczkowska, J.; Penc, B.; Bergues, B.; Kowalski, K.; Rysz, J.; Janik, J. *Macromolecules* **2003**, *36*, 4060−4067.
(32) Walheim, S.; Ramstein, M.; Steiner, U. *Langmuir* **1999**, *15*, 4828−4836.
(33) Cyganik, P.; Budkowski, A.; Raczkowska, J.; Postawa, Z. *Surf. Sci.* **2002**, *507−510*, 700−706.
(34) Reifer, D.; Windeit, R.; Kumpf, R. J.; Karbach, A.; Fuchs, H. *Thin Solid Films* **1995**, *264*, 148−152.
(35) Thomann, Y.; Suhm, J.; Thomann, R.; Bar, G.; Maier, R.-D.; Mülhaupt, R. *Macromolecules* **1998**, *31*, 5441−5449.
(36) Nysten, B.; Legras, R.; Costa, J.-L. *J. Appl. Phys.* **1995**, *78*, 5953−5958.
(37) Labardi, M.; Allegrini, M.; Marchetti, E.; Sgarzi, P. *J. Vac. Sci. Technol. B* **1996**, *14*, 1509−1512.

(38) Tomasetti, E.; Legras, R.; Nysten, B. *Nanotechnology* **1998**, *9*, 305−315.
(39) Swaminathan, K.; Marr, D. W. M. *J. Appl. Polym. Sci.* **2000**, *78*, 452−457.
(40) Tanem, B. S.; Kamfjord, T.; Augestad, M.; Løvgren, T. B.; Lundquist, M. *Polymer* **2003**, *44*, 4283−4291.
(41) Galuska, A. A.; Poulter, R. R.; McElrath, K. O. *Surf. Interface Anal.* **1997**, *25*, 418−429.
(42) Pfau, A.; Janke, A.; Heckmann, W. *Surf. Interface Anal.* **1999**, *27*, 410−417.
(43) Said, M. A.; Balik, C. M.; Carlson, J. D. *J. Polym. Sci., Part B: Polym. Phys.* **1988**, *26*, 1457−1467.
(44) Musumeci, P.; Calcagno, L.; Percolla, R.; Foti, G. *J. Appl. Phys.* **1995**, *77*, 3766−3773.
(45) Calcagno, L. *Nucl. Instrum. Methods B* **1995**, *105*, 63−70.
(46) Koval, Y. *J. Vac. Sci. Technol. B* **2004**, *22*, 843−851.
(47) Kudoh, H.; Sasuga, T.; Seguchi, T. *Radiat. Phys. Chem.* **1997**, *50*, 299−302.
(48) Schnabel, W.; Klaumünzer, S.; Sotobayashi, H.; Asmussen, F.; Tabata, Y. *Macromolecules* **1984**, *17*, 2108−2111.
(49) Schnabel, W.; Klaumünzer, S. *Radiat. Phys. Chem.* **1991**, *37*, 131−134.
(50) Schnabel, W.; Klaumünzer, S. *Radiat. Phys. Chem.* **1989**, *33*, 323−328.
(51) Calcagno, L.; Foti, G.; Licciardello, A.; Puglisi, O. *Appl. Phys. Lett.* **1988**, *53*, 1495−1497.
(52) Calcagno, L.; Foti, G.; Licciardello, A.; Puglisi, O. *Appl. Phys. Lett.* **1988**, *53*, 907−909.
(53) Calcagno, L.; Percolla, R.; Masciarelli, D.; Foti, G. *J. Appl. Phys.* **1993**, *74*, 7572−7576.
(54) Merhari, L.; Belorgeot, C.; Moliton, J. P. *J. Vac. Sci. Technol. B* **1991**, *9*, 2511−2522.
(55) Terrasi, A.; Foti, G.; Hwu, Y.; Margarirondo, G. *J. Appl. Phys.* **1991**, *70*, 1885−1887.
(56) Beamson, G.; Clark, N. W.; Hayes, N. W.; Law, D. S.-L.; Siracusa, V.; Recca, A. *Polymer* **1996**, *37*, 379−385.
(57) Lewis, M.; Lee, B. H. *J. Nucl. Mater.* **1993**, *203*, 224−232.
(58) Calcagno, L.; Compagnini, G.; Foti, G. *Nucl. Instrum. Methods B* **1992**, *65*, 413−422.
(59) Davenas, J.; Thevenard, P.; Boiteux, G.; Fallavier, M.; Lu, X. L. *Nucl. Instrum. Methods B* **1990**, *46*, 317−323.
(60) Marletta, G. *Nucl. Instrum. Methods B*, **1990**, *46*, 295−305.
(61) Ektessabi, A. M.; Sano, T. *Rev. Sci. Instrum.* **2000**, *71*, 1012−1015.
(62) White, H.; Pu, Y.; Rafailovich, M.; Sokolov, J.; King, A. H.; Giannuzzi, L. A.; Urbanik-Shannon, C.; Kempshall, B. W.; Eisenberg, A.; Schwarz, S. A.; Strzhemechny, Y. M. *Polymer* **2001**, *42*, 1613−1619.
(63) Aubry, C.; Trigaud, T.; Moliton, J. P.; Chiron, D. *Synth. Met.* **2002**, *127*, 307−311.
(64) Magerle, R. *Phys. Rev. Lett.* **2000**, *85*, 2749−2752.
(65) Bernasik, A.; Rysz, J.; Budkowski, A.; Kowalski, K.; Camra, J.; Jedlinski, J. *Macromol. Rapid Commun.* **2001**, *22*, 829−834.
(66) Saltikov, S. A. *Proceedings of the 2nd International Congress for Stereology*; Helias: New York, 1967.

MA0482664